Bacteriophage tailspikes and bacterial O-antigens as a model system to study weak-affinity protein-polysaccharide interactions

Yu Kang[1,‡,†] , Ulrich Gohlke[2,‡], Olof Engström[3,‡], Christoffer Hamark[3], Tom Scheidt[4,§], Sonja Kunstmann[4], Udo Heinemann[2,5], Göran Widmalm[3], Mark Santer[1,*] and Stefanie Barbirz[4,*]

[1]Max Planck Institute of Colloids and Interfaces, Am Mühlenberg 1, 14476 Golm, Germany.
[2]Max-Delbrück-Centrum für Molekulare Medizin in der Helmholtz-Gemeinschaft, Robert-Rössle-Str. 10, 13125 Berlin, Germany.
[3]Department of Organic Chemistry, Arrhenius Laboratory, Stockholm University, S-106 91 Stockholm, Sweden.
[4]Physikalische Biochemie, Universität Potsdam, Karl-Liebknecht-Str. 24-25, 14476 Potsdam, Germany.
[5]Institut für Chemie und Biochemie, Freie Universität, Takustr. 6, 14195 Berlin, Germany.

Supporting Information

ABSTRACT: Understanding interactions of bacterial surface polysaccharides with receptor protein scaffolds is important for the development of antibiotic therapies. The corresponding protein recognition domains frequently form low-affinity complexes with polysaccharides that are difficult to address with experimental techniques because of the conformational flexibility of the polysaccharide. In this work, we studied the tailspike protein (TSP) of the bacteriophage Sf6. Sf6TSP binds and hydrolyzes the high-rhamnose, serotype Y O-antigen polysaccharide of the Gram-negative bacterium *Shigella flexneri* (*S. flexneri*) as a first step of bacteriophage infection. Spectroscopic analyses and enzymatic cleavage assays confirmed that Sf6TSP binds long stretches of the *S. flexneri* O-serogroup Y polysaccharide. Crystal structure analysis and saturation transfer difference (STD) NMR spectroscopy using an enhanced method to interpret the data permitted the detailed description of affinity contributions and flexibility in an Sf6TSP-octasaccharide complex. Dodecasaccharide fragments corresponding to three repeating units of the O-antigen in complex with Sf6TSP were studied computationally by molecular dynamics simulations. They showed that distortion away from the low-energy solution conformation found in the octasaccharide complex is necessary for ligand binding. This is in agreement with a weak-affinity functional polysaccharide-protein contact that facilitates correct placement and thus hydrolysis of the polysaccharide close to the catalytic residues. Our simulations stress that the flexibility of glycan epitopes together with a small number of specific protein contacts provide the driving force for Sf6TSP-polysaccharide complex formation in an overall weak-affinity interaction system.

INTRODUCTION

In the bacterial cell, polysaccharide-protein interactions play a significant role from formation of structural components of the cell wall to functions in metabolic pathways. For example, polysaccharides interact with proteins of the bacterial glycan synthesis and the export apparatus transferring them to the outer membrane leaflet or into extracellular space.[1] Furthermore, polysaccharide-protein complexes are found in interactions with host immune systems[2], during biofilm formation[3], and in pathogenesis, which emphasizes the important role of bacterial polysaccharides as vaccine targets.[4] In contrast to their ubiquitous relevance in biology, descriptions of these complexes on a molecular level are scarce. Polysaccharide repeat units (RUs) in complex with antibodies have been analyzed with X-ray crystallography, molecular dynamics (MD) simulations and NMR spectroscopy.[5-6] The complex of a biofilm forming exopolysaccharide with a periplasmic transporter was characterized by X-ray crystallography and subsequent simulation of monosaccharide building blocks along an extended binding groove.[7] However, in most cases studied, rather short oligosaccharides (*i.e.* up to hexamers) were observed in direct contact to the protein, and so far only one decasaccharide and another

Scheme 1: Repeat structure of *Shigella flexneri* serogroup Y O-polysaccharide[a]

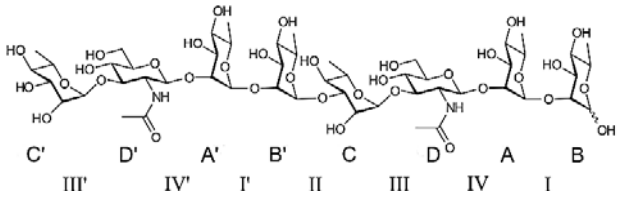

[a] Two repeat units of the *Shigella flexneri* O-serogroup Y polysaccharide antigen with the sequence [→3)-α-L-Rha*p*-(1→3)-β-D-GlcNAc*p*-(1→2)-α-L-Rha*p*-(1→2)-α-L-Rha*p*-(1→]$_2$. Capital letters CDAB label monosaccharides, roman numerals glycosidic linkages as described elsewhere.[9]

dodecasaccharide complex have been described.[6,8] With growing chain length, the number of possible conformations increases quickly, and intramolecular H-bond formation may favor the occurrence of glycan secondary structure leading to a number of conformational epitopes.[9] Accordingly, the characterization of longer saccharide chains has to rely on a combination of experimental techniques and computer simulations.[10,11]

As part of the bacterial cell surface, polysaccharides are also a receptor for bacteriophages. Certain bacteriophages specifically recognize the O-antigen polysaccharide of Gram-negative bacteria using tailspike proteins (TSP).[12] TSP attain specificity via long and shallow binding grooves, and several complexes of TSP with oligosaccharide fragments up to nonamer length have been described. [13-14] The Gram-negative bacterium *Shigella flexneri* (*S. flexneri*) causes bacillary dysentery with high mortality in infants in countries with low medical standards, and it therefore is an important vaccine target.[15] Most of the infective strains share a similar O-antigen with a polyrhamnose backbone. In this work, we have analyzed the binding of the O-antigen polysaccharide of *S. flexneri* to TSP of the bacteriophage Sf6 (Sf6TSP) to examine how extended polysaccharide chains interact specifically with a protein surface. The O-antigen consists of a carbohydrate backbone with high (75 %) rhamnose content, and a growing body of evidence suggests that this specific composition gives rise to highly flexible, dynamic polymers.[16,17] Virulence of *S. flexneri* is intimately linked to this specific and dynamic O-antigen composition.[8,18] The basic unbranched serogroup Y antigen is composed of tetrasaccharide repeat units (RU) with the structure →2)-α-L-Rha*p*-(1→2)-α-L-Rha*p*-(1→3)-α-L-Rha*p*-(1→3)-β-D-GlcNAc*p*-(1→ (Scheme 1).[19] Sf6TSP recognizes specifically this O-antigen polysaccharide and cleaves the α-1,3 glycosidic bond between two rhamnose units, producing oligosaccharides.[20,21] Sf6TSP forms a homotrimeric complex (M_W = 166 kDa) with a parallel β-helix architecture and three O-antigen binding sites located in long grooves at the subunit interfaces.[22] In the present work, we have analyzed Sf6TSP in the presence of polysaccharide fragments of different length and used a thorough experimental description as the starting point for computer simulations of long glycan fragments on the protein surface. We found that in the overall weak-affinity Sf6TSP polysaccharide interaction system specific protein contacts as well as the high flexibility of the binding partners are a prerequisite for complex formation.

RESULTS

Crystal structure analysis. Diffracting crystals were obtained for various complexes of Sf6TSP with octa-, dodeca- and lipopolysaccharides of *S. flexneri* O-serogroup Y. Only for the double mutant Sf6TSP E366A/D399A ($Sf6TSP_{mut}$), which is catalytically inactive[22] (Figure S1 the Supporting Information), an octasaccharide ligand could be observed in the binding site (Figure 1A and Figure S2 in the Supporting Information) using a 1.95 Å resolution data set with space group $P2_1$ with six $Sf6TSP_{mut}$ chains per asymmetric unit (see Supporting Information for all crystallographic data). The previously described wild-type protein ($Sf6TSP_{WT}$) had been crystallized in space group R3 with one molecule per asymmetric unit.[22] Analysis of the atomic displacement factors (ADF) showed

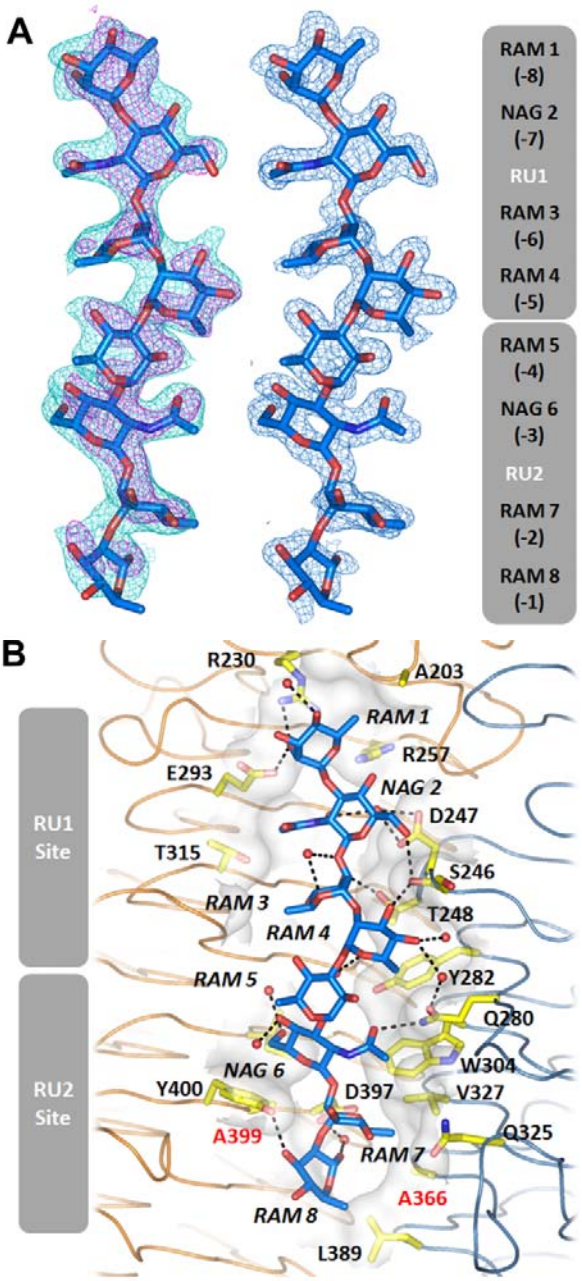

Figure 1. Figure caption. (A) Crystal structure of *Shigella flexneri* O-serogroup Y octasaccharide bound to $Sf6TSP_{Mut}$. (Left) Initial m|Fo|-D|Fc| electron density (red, 2.5 σ) and non-crystallographic-symmetry (NCS)-averaged m|Fo|-D|Fc| electron density (green, 2.0 σ). After refinement, six ligand molecules in the asymmetric unit superimposed with a root mean square deviation (rmsd) of 0.30 Å. (Right) 2m|Fo|-D|Fc| electron density (blue) after refinement (1.0 σ). The building blocks of RU1 and RU2 are defined as RAM (α-L-rhamnose) and NAG (N-acetyl- β-D-glucosamine). (B) Binding site of the $Sf6TSP_{Mut}$/octasaccharide complex between two subunits (orange and blue). RAM8 represents the reducing end of the octasaccharide. RU1 and RU2 sites mark the position of the repeating units 1 and 2, respectively, of the octasaccharide. 19 direct or water-mediated H-bonds are formed between ligand and protein. A366 and A399 are the mutated catalytic residues Glu and Asp, respectively.

increasing flexibility of the monosaccharide units towards the reducing end, where in one of the octasaccharides the $^{3}S_{1}$ ring conformation was found for the terminal rhamnose instead of the anticipated $^{1}C_{4}$ conformation (see Figure S3 in the Supporting Information). The overall architecture of ligand-bound Sf6TSP$_{mut}$ is identical with respect to ligand-free Sf6TSP$_{WT}$ (rmsd = 0.33 Å). The binding pocket of the Sf6TSP$_{mut}$-octasaccharide complex consists of a large groove formed by adjacent β-helix domains of different subunits in the trimer. The binding groove accommodates 2RU of O-antigen in the RU1 and RU2 sites (Figure 1B) flanked by the catalytic residues E366 and D399.[22] RU1 of the oligosaccharide forms a total of six direct H-bonds, one water-mediated H-bond, as well as three hydrophobic interactions with nine amino-acid residues in total (RU1 site). RU2 follows the binding groove with fewer polar interactions than RU1 (two direct, one water-mediated H-bond), but with three hydrophobic interactions (RU2 site). Overall, fifteen ordered water molecules were found in H-bonding distance to the ligand.

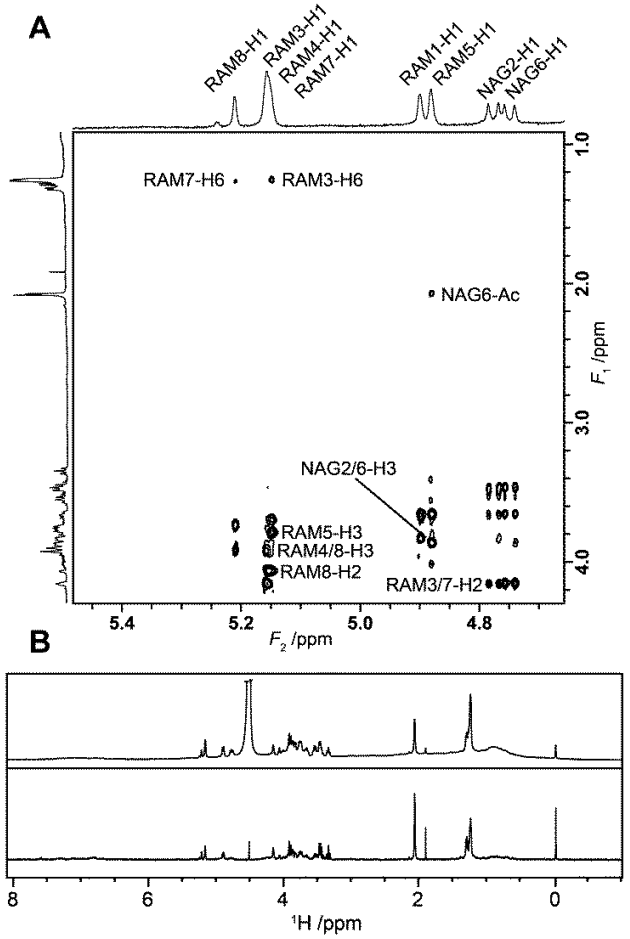

Figure 2. Figure caption. (A) ^{1}H,^{1}H-trNOESY spectrum with selected inter-glycosidic cross-peaks annotated. (B) ^{1}H NMR spectrum (top) and a STD spectrum (bottom) of Sf6TSP with the octasaccharide in D_2O. The irradiation frequency in the STD experiment was set to 7 ppm, and the saturation time was 2 s.

NMR studies of S. flexneri O-serogroup Y octasaccharide bound to Sf6TSP. We analyzed the Sf6TSP$_{mut}$-octasaccharide complex in a 2D ^{1}H,^{1}H-trNOESY experiment (for the ^{1}H NMR characterization of the free ligand in solution see Table S3 in the Supporting Information). The bound octasaccharide showed the strongest inter-glycosidic cross-peaks from anomeric protons to protons on glycosyloxylated carbons (*e.g.* H2 or H3) for each glycosidic linkage (Figure 2A), as would be anticipated for an all-*syn* conformation.[23] Additional transglycosidic trNOEs were found between RAM5-H1 and NAG6-Ac, but not for the corresponding protons in RU1, which can be explained by a shorter distance between the spins in RU2. Likewise, a cross-peak was found in a spectral overlap region; due to its shape it was assigned to a correlation between the methyl group in NAG2-Ac and RAM1-H2. For RU2 the corresponding cross-peak was missing. These results are in agreement with a change between the ϕ1 and ϕ5 torsion angles of 9 °- 15 ° as well as 15 °- 20 ° for the Ψ1 to Ψ5 torsion angles, as seen in the crystal structure and in the MD simulations (see below and Supporting Information). The *N*-acetyl groups also show transglycosidic trNOEs to the H4 protons of RAM3 and RAM7. Furthermore, trNOEs were observed for the methyl groups of RAM3, RAM7 and RAM4 to RAM4-H1, RAM8-H1 and RAM5-H2. Together with the absence of transglycosidic trNOEs from any of the methyl groups of RAM1 and RAM5, all results from trNOESY-NMR are in good agreement with the bound octasaccharide conformation seen in the crystal structure. ^{1}H saturation transfer difference (STD) NMR experiments were performed (Figure 2B) and initial slopes of STD amplification factor build up curves (STD-AF$_0$) were calculated (see tabulated values in the Supporting Information). The methyl group of RAM4 has the highest STD-AF$_0$ when saturating aromatic protein residues, which is in agreement with the crystal structure where it is buried in the protein in close proximity to Tyr282. The second strongest STD-AF$_0$ is the average of RAM3-H4 and RAM7-H4, of which the latter is adjacent to Trp304. The absence of aromatic residues is more profound at the non-reducing end of the binding pocket, and this is reflected in the lower STD-AF$_0$ values for NAG2-Ac compared to NAG6-Ac. A particularly weak STD-AF$_0$ found forRAM5 may be explained by a longer distance to the protein surface for this residue due to the pucker in the saccharide chain (see Figure S4 in the Supporting Information).

Molecular dynamics simulations. We started simulations of Sf6TSP in complex with tetrasaccharide fragments (Figure 3A), with the protein kept at the geometry of the X-ray structure. During MD runs of at least 100 ns length, tetrasaccharides remained stable in the RU1 site -2 reproducing the binding mode found in the crystal structure including some of the structural water molecules.[22] The bound tetrasaccharide assumes the solution conformer close to the global free-energy minimum. Also, an octasaccharide resided stably in the binding site during MD simulations, both in the Sf6TSP$_{WT}$ and Sf6TSP$_{mut}$ in a conformation similar to those observed in the X-ray structure (Figure 3B). The H-bond pattern found in the crystal structure was well reproduced showing that the octasaccharide was mainly fixed in the binding site via RAM1, RAM3 and RAM8. Average torsion angles within RU1 of the bound octasaccharide settle in the same energy minima as in RU2 (Figure 3C and Tables S5 and

S6 in the Supporting Information). Rmsd values of monosaccharide positional variations increased from 0.9 Å at the non-reducing end to 2.6 Å at the reducing end in agreement with increased atomic displacement factors found in the crystal structure.

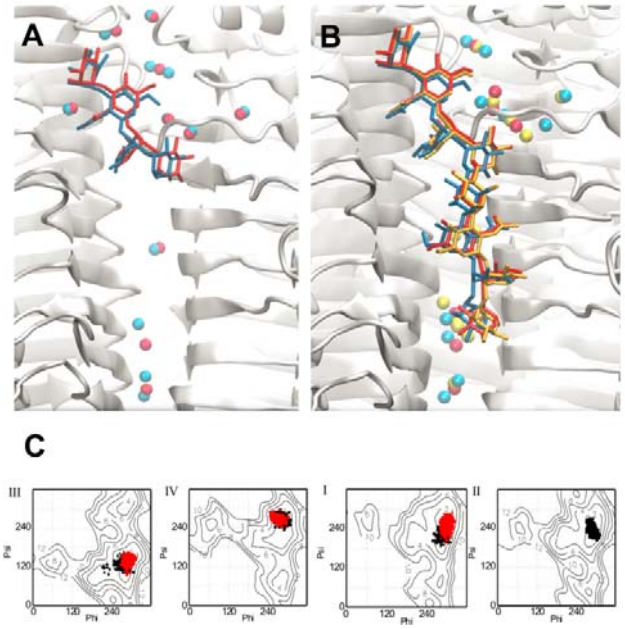

Figure 3. Figure caption. MD simulations of Sf6TSP oligosaccharide complexes. obtained with Amber/Glycam force fields. (A) Tetrasaccharide complex with Sf6TSP wild type (red) in comparison with position in the crystal structure (blue; pdb:2VBM). (B) Octasaccharide complex with Sf6TSP wild type (red) or mutant E366A/D399A (yellow) in comparison with position in the crystal structure of the mutant E366A/D399A (blue; pdb:4URR). (C) ϕ-Ψ-distributions of the octasaccharide bound to Sf6TSP. Black and red dots represent the ϕ-Ψ distributions of site -2 and site -1, respectively. Free energies were calculated for linkages I,II, III and IV (*cf.* Scheme 1) in disaccharides as described previously.[17] Linkage II is only present in the octasaccharide. For a comparison of torsion angle distributions see Table S5 in the Supporting Information.

Simulation of STD-NMR build-up curves using a novel modified CORCEMA approach accounting for chemical shift dispersion (CSD) in large proteins. In order to further validate the X-ray and computational protein-ligand models we simulated STD-AF build-up curves by employing a complete relaxation and conformational exchange matrix (CORCEMA).[24] Sf6TSP is a trimeric protein complex with a molecular weight of 165 kDa. To describe the magnetic saturation of this large protein-ligand complex accurately, the chemical shift dispersion (CSD) caused by rapid transverse relaxation had to be considered. In the resulting CORCEMA-ST-CSD approach the NMR line shapes influenced by the transverse relaxation time T_2 were taken into account by looping the CORCEMA-ST program for narrow intervals (n) over the whole spectrum. Concomitantly, relative contributions to the spectral intensity within the defined irradiation bandwidth ($X_{sat,n}$) were calculated for protons in the binding site and with chemical shifts within an interval n (Scheme 2; for full description of the CORCEMA-ST-CSD analysis see the Supporting Information). The simulated CORCEMA-ST output for each interval n ($STD\text{-}AF_{CORCEMA\text{-}ST,n}$) was multiplied with the corresponding $X_{sat,n}$ and the sum over all n reported as the final simulated result ($STD\text{-}AF_{sim}$, equation 1).

$$STD\text{-}AF_{sim} = \sum_{n=1}^{N} X_{sat,n} \cdot STD\text{-}AF_{CORCEMA\text{-}ST,n} \qquad (1)$$

Simulated STD-AF showed good agreement with experimental values when the average ligand atomic coordinates from the MD trajectory were evaluated with an R_{NOE} between 0.32 and 0.53. When using the ligand model from the crystal structure, good agreement with the experiment was only found for $STD\text{-}AF_{sim}$ from resonances at the non-reducing end (Figure 4A). By contrast, $STD\text{-}AF_{sim}$ of RAM8 deviated from experimental STD-AF significantly (Figure 4B). These results emphasize the dynamic nature of the reducing end and show that MD simulations fully accounted for the octasaccharide dynamics experimentally observed in the binding site, whereas the crystal structure accounted for the observed reducing end flexibility only by showing increased atomic displacement factors.

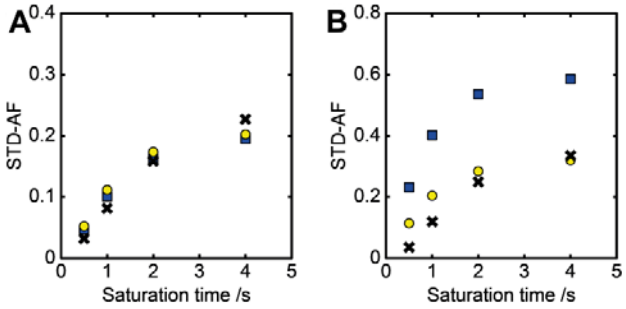

Figure 4. Figure caption. CORCEMA-ST-CSD simulated STD-AF for RAM1-H1 (A) or RAM8-H1 (B) anomeric resonances. Ligand coordinates used from molecular dynamics simulations (yellow circles) and X-ray ligand B (blue squares) compared to experimental STD-AF (crosses).

Scheme 2: The CORCEMA-ST-CSD approach[b]

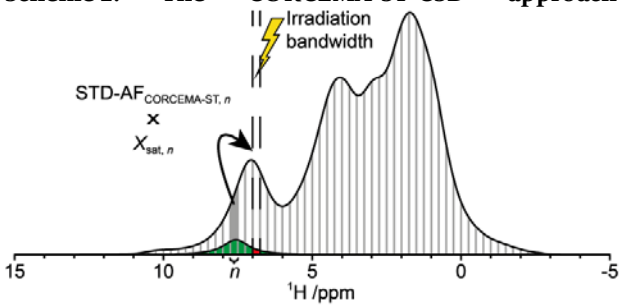

[b] Simulated ^{1}H NMR spectrum of $Sf6TSP_{mut}$ with protons within an irradiation bandwidth between 6 to 7 ppm depicted separately (in front). Green: protons with chemical shifts within the irradiation bandwidth that are still within the irradiation bandwidth. Blue: protons with chemical shifts within the irradiation bandwidth that populate parts of the spectrum beyond the irradiation bandwidth due to relaxation.

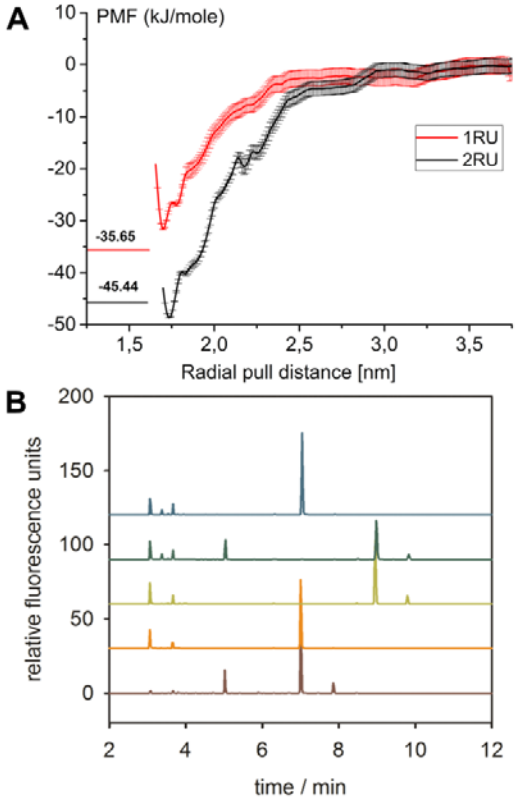

Figure 5. Figure caption. (A) Potential of mean force (PMF) curves for tetrasaccharide (score -36 kJ mol^{-1}, red) and octasaccharide (score -45 kJ mol^{-1}, black) Sf6TSP complex formation. As reference the highest scores obtained by docking are given as horizontal lines. (B) Sf6TSP cleavage products of *Shigella flexneri* serogroup Y oligosaccharides or lipopolysaccharide (LPS). Samples were analyzed by capillary electrophoresis with laser-induced fluorescence detection (CE-LIF) after fluorophore labeling. From bottom to top: LPS cleavage products, octasaccharide control, dodecasaccharide control, dodecasaccharide with fluorescence label at the reducing end incubated with Sf6TSP, octasaccharide incubated with Sf6TSP.

Determinants of affinity in the Sf6TSP binding site. Aromatic as well as glutamate residues near the ligand are underrepresented in Sf6TSP when compared with rhamnose- or *N*-acetylglucosamine-binding proteins (see Figure S10 in the Supporting Information). Together with the small number of ligand-protein contacts observed this points to low octasaccharide affinity. In fact, attempts to quantify the affinity of complex formation with isothermal titration calorimetry failed and we could only estimate the dissociation constants for the Sf6TSP-octasaccharide complex to lie in the mM range. Using docking, the binding poses from x-ray analysis were recognized as low-energy, (Figure 5A). Potential of mean force calculations by umbrella sampling showed that energies needed to pull tetra- or octasaccharides to large radial distances agreed well with the free energies obtained from docking which illustrates that adding the second repeat unit increased the binding affinity only moderately. This agrees with the finding that the H-bond network fixing the octasaccharide in the Sf6TSP binding groove is mainly located at the RU1 site. Mutation of residues in the RU1 site drastically increased octasaccharide flexibility in the binding groove and illustrates its important role in generating specificity (Figure S11 in the Supporting Information). Given that the catalytic residues are located at the C-terminal end of the binding groove next to the RU2 site, this binding mode must also influence the size of polysaccharide cleavage products. After Sf6TSPΔN_{WT} lipopolysaccharide (LPS) hydrolysis we indeed only found the octasaccharide as the main product (Figure 5B), in agreement with at least the RU1, RU2 and an additional RU3 site occupied during cleavage. By contrast, starting with octasaccharide as educt, it was not cleaved into tetrasaccharides, even after several days of incubation with Sf6TSP, whereas tetrasaccharides could be produced from the dodecasaccharide.[21] This further corroborates that also the RU2 site has to be occupied for successful cleavage and probably contributes most to substrate affinity.

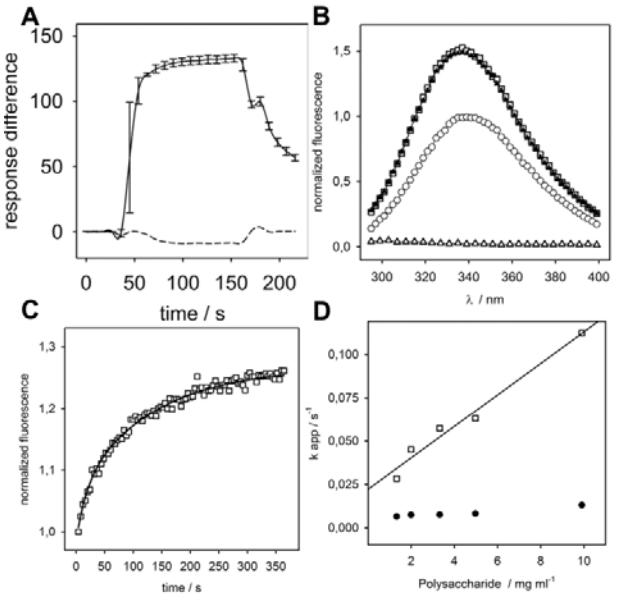

Figure 6. Figure caption. *S. flexneri* serogroup Y polysaccharide binding to Sf6TSP. (A) Surface plasmon resonance (SPR) response upon binding of Sf6TSP (100 µg ml^{-1}) of cleavage-deficient mutant D399A to immobilized LPS (solid) or to immobilized LPS enzymatically pretreated with Sf6TSP wild type (dashed) Error bars represent standard deviations from three injections at 25 °C. (B) Normalized protein fluorescence spectra of 184 nM Sf6TSP E366A/D399A in the absence (open circles) or presence of 33.2 µg ml^{-1} (open squares) or 66.2 µg ml^{-1} (filled triangles) polysaccharide. Control: 66.2 µg ml^{-1} polysaccharide without protein (open triangles). (C) Relaxation to binding equilibrium at 10 °C upon manually mixing 184 nM Sf6TSP E366A/D399A with 33.2 µg ml^{-1} polysaccharide (open squares) described by a biexponential model with k_1 = 5.73±0.94·10^{-2} s^{-1} and k_2 = 0.76±0.04·10^{-2} s^{-1} (solid line). (D) Concentration dependence of apparent rate constants k_{app}. of slow (filled circles) and fast (open squares) kinetic phases. A polysaccharide dissociation rate constant of 0.022±0.003 s^{-1} was determined from the linear fit of the fast phase as described elsewhere.[25]

Binding studies of Sf6TSP with long O-antigen fragments. Polysaccharide interactions of Sf6TSP were analyzed on surface-immobilized LPS preparations of *S. flexneri* serogroup Y with surface plasmon resonance (Figure 6A). To prevent polysaccharide cleavage, the catalytically inactive Sf6TSPD399A mutant was used. The protein specifically bound to long O-antigen chains, but was unable to recognize LPS preparations that were pretreated enzymatically with $Sf6TSP_{WT}$ to cleave off the O-polysaccharide from the surface. We can therefore exclude that LPS core- or lipid A-moieties interact with Sf6TSP. Rather; the long O-antigen chains on intact LPS are required for stable interaction. Moreover, dissociation off-rates from the LPS surface were comparable to those measured as protein fluorescence signal relaxation rates obtained upon manual mixing with polysaccharide preparations of different concentrations (Figures 6B-D and Figure S12 in the supporting information). Off-rates of similar magnitude were also found for dissociation of a *Salmonella* O-antigen polysaccharide from bacteriophage P22 TSP.[12] By contrast, no fluorescence signal change was detectable upon mixing with octa- or dodecasaccharides. We therefore wanted to obtain a molecular description of a Sf6TSP binding mode for ligands longer than an octasaccharide and extended our MD analysis to dodecasaccharides to explore possible binding modes of longer chains. We simulated a fragment of three RU by extending the octasaccharide by another repeating unit into a putative RU3 site located beyond the catalytic residues. However, simple extension of the octasaccharide by another RU while keeping its initially bound position and staying close to a minimum-energy conformation was hindered by steric clashes (see Figure S13 in the Supporting Information). To avoid the latter, a high-energy starting conformation had to be chosen with RU3 rotated around linkage II into a state of torsion about 7 kcal mol^{-1} above the global minimum for that linkage.[17] Irrespective of whether the Glycam/Amber or the CHARMM force field was used, in subsequent MD runs all glycosidic torsions rapidly adjusted within 10 ps to low energy conformations. As initial result, the dodecasaccharide settled in an elongated pose into the binding groove for a period of up to 10 ns. However, during the further simulation time RU1 and RU2 permanently detached from the canonical octasaccharide binding site (see Figures S14 and S 15 in the Supporting Information). With Amber/Glycam, RU1 and RU2, although displacing, stayed in contact with the TSP surface, whereas RU3 was fixated from the beginning through H-bonds between Asn455 and Ram11, Arg364 and NAG10, and RAM12 and Asn508RU3, respectively. By contrast, in the CHARMM case, the dodecasaccharide soon detached from the groove and temporarily from TSP surface, and assumed its final pose. Furthermore, in a second set of simulations, we enhanced protein flexibility and released all restraints from the protein backbone in the β-strand-connecting loops. This seems a reasonable assumption for the protein dynamics at ambient temperature, and all subsequent simulations showed that this did not affect the global shape of Sf6TSP as all protein C-α positions stayed close to those found in the crystal structure. Using Amber/Glycam, the dodecasaccharide now quickly relaxed into an elongated pose with its first two RUs largely following the orientation of the octasaccharide in the crystal structure (Figure 7A-D), whereas RU3 took a similar position to that seen in the simulations with restrained loop backbones but with more stably occupied H-bonds (Figure 7E and Table S6 in the Supporting Information). Also in the CHARMM simulations with flexible loops the ligand was firmly accommodated along the groove, but showed more conformational flexibility than in the Amber/Glycam simulations (Figure 7F). Especially RU3 was still dynamically moving back and forth between the two walls of the binding groove illustrated by a lower H-bond occupancy (see Figure S14 and Table S6 in the Supporting Information).

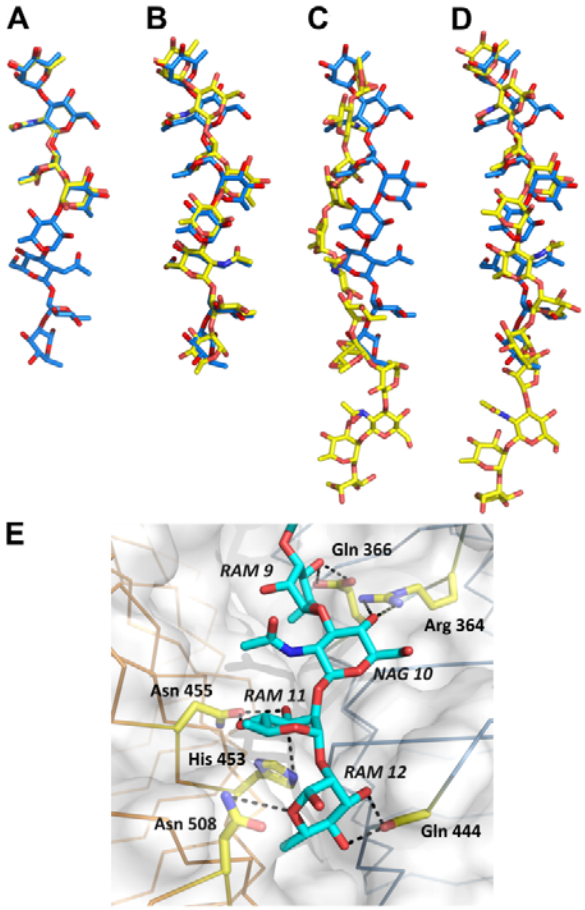

Figure 7. Figure caption. Superimposition of *S. flexneri* serogroup Y octasaccharide model in complex with Sf6TSP from crystal structure (blue) with molecular dynamics simulation models (yellow) of (A) tetrasaccharide (RU1), (B) octasaccharide (RU1, RU2), (C) dodecasaccharide (RU1, RU2, RU3) in presence of fully restrained protein backbone, (D) dodecasaccharide in presence of unrestrained protein loop regions. (E) Binding site of RU3 in the Sf6TSP-dodecasaccharide complex between two subunits (orange and blue) shown for the unrestrained protein backbone simulation.

DISCUSSION

Sf6TSP as an example for weak-affinity polysaccharide binding. Carbohydrate ligands become more flexible with increasing length, resulting in weak affinities challenging the understanding of how polysaccharides bind to proteins transiently. For example, in processes such as polysaccharide synthesis and hydrolysis[26], chain length control[27] or transport[28], short-lived polysaccharide binding may take

place with rapid ligand off-rates. The computational approach fills the gap between the experimentally accessible descriptions of small oligosaccharides in protein binding sites and the need for models of large protein-polysaccharide complexes.[10,29] The Sf6TSP analyzed in this work is a polysaccharide hydrolyzing enzyme. It recognizes and cleaves the specific O-antigen part of LPS as the first step of the bacteriophage Sf6 infection cycle in order to penetrate the protective polysaccharide coat of the bacteria and reach outer membrane receptors[30]. The bacteriophage is equipped with six TSP and hence displays 18 polysaccharide binding sites to assure multivalent fixation on the bacterial cell surface, whereas TSP hydrolysis and rebinding enable receptor search and lateral movement of the phage across the membrane LPS layer. The Sf6TSP glycan binding groove only offers a limited number of H-bonding contacts providing specificity while hydrophobic patches are lacking, resulting in an overall weak-affinity polysaccharide interaction system.

Experimental and computational methods to describe glycan ligand flexibility in Sf6TSP complexes. Sf6TSP-octasaccharide complexes showed flexibility at the glycan reducing end. In many cases, ligand flexibility is not well resolved in crystal structures due to averaging over atom positions by crystallographic symmetry. Also in a previous study, electron density was only found for the tetrasaccharide in site -2 when $Sf6TSP_{WT}$ crystallized in a space group of higher symmetry[22]. However, the $Sf6TSP_{Mut}$ octasaccharide complex forms a crystallographic asymmetric unit with two TSP trimers. This produced six distinct snapshots of ligand conformations preserved upon cooling from ambient to cryo temperatures and thus captured the flexibility of the octasaccharide reducing end. MD simulations in combination with build-up rates found with STD-NMR at 56 °C provided a dynamic picture of this flexibility. Nevertheless, a potential difficulty with this and NMR analyses in general is that polysaccharide binding may involve large interaction surfaces. The analysis of high molecular weight protein-ligand complexes sets limits to quantitative STD-NMR analyses in cases where the irradiation frequency interval does not fully cover the chemical shifts of certain protein resonances, resulting in only partially saturated signals. Yet, the simulation of STD-AF build-up curves with classical CORCEMA-ST relies on precise chemical shifts.[24,31] Predicting chemical shifts computationally is sometimes inaccurate; however, in the expanded CORCEMA-ST-CSD approach used in this work to analyze STD data from Sf6TSP-oligosaccharide complexes, chemical shifts are described as distributions rather than as discrete signals and thus less sensitive to the chosen irradiation interval in the corresponding simulation. In addition, all results were calculated directly from estimated physical parameters (*e.g.* $\tau_{C\text{-protein}}$, $\tau_{C\text{-ligand}}$, K_D *etc.*) without any major parameter optimization. This is in contrast to the high number of input parameters used in CORCEMA-ST that may result in forced fitting scenarios. Hence, in the present study, NMR spectroscopy and X-ray crystallography provided robust validation of the computational descriptions of TSP O-antigen binding. This emphasizes the improvement in the quality of carbohydrate force fields due to specifically adapted glycan parametrization procedures.[32,33] MD simulations in this work indeed produced similar results when calculated with either the CHARMM or GLYCAM force field, especially for the dynamics at the octasaccharide reducing end. Slightly different H-bond occupancies or minor distance fluctuations were observed, however, the spread in these observables can be seen in analogy to the experimental uncertainty.

For the dodecasaccharide by contrast, positional dynamics and flexibility were enhanced when calculated with CHARMM, particularly for RU3. One might thus speculate that although both force fields showed similar results in most simulations, glycans in Glycam simulations may have a more pronounced tendency to stick to protein surfaces described by Amber03 (see Figures S14 and S15 in the Supporting Information). The precise origin of this discrepancy is yet to be elucidated, but it seems reasonable to regard these two dynamical behaviors as the outer limits of accuracy in the actual description. Reliable computational descriptions of protein-carbohydrate complexes furthermore are a prerequisite to exactly define water molecules in binding sites. MD simulations in this study showed good agreement of water positions with those in the crystal structure (*cf.* Figure 3). However, the fundamental challenge remains in assigning desolvation penalties to individual water molecules in order to predict binding affinities from simulation data.

Computational simulation of binding of long polysaccharide fragments to Sf6TSP. In this work, the thorough experimental description of octasaccharide binding to Sf6TSP and the excellent agreement with data from MD simulations is prerequisite for the definition of a plausible computational setup that finds binding modes of dodecasaccharide fragments. It should be emphasized that no experimental evidence of a dodecasaccharide pose is yet available; soaking of Sf6TSP crystals with dodecasaccharide, polysaccharide or lipopolysaccharide, for instance, had not shown any interpretable ligand electron density, as ligand flexibility is likely to cause disorder in the crystal. For the octasaccharide ligand, the experiments clearly emphasized the enhanced flexibility of RU2. This suggests that RU2 and RU3 have enough freedom to adapt their conformation while choosing a high energy dodecasaccharide starting conformer that avoids steric clashes. At the same time, fixing RU1 in the RU1 site is required. This finding is corroborated by the observation that mutations of H-bond providing residues E293 and D247 in the RU1 site had previously shown a reduced hydrolysis turnover[22], stressing that the corresponding protein-ligand H-bonds are important to position the polysaccharide fragments correctly for cleavage. In the computational setup, the backbone of the protein loops had to be made fully flexible to establish all contacts in the -2 site correctly, whereas contacts in site +1 were similar irrespective of protein loop flexibility. In combination with a high-energy dodecasaccharide starting conformer in the simulation this helps to overcome local barriers presented by the protein scaffold and to sample conformations slightly elevated in energy in order to arrive at the final pose. Limits to this model come from the fact that in this study only one high energy dodecasaccharide starting structure was used. With the high energy starting conformation the sampling of possible final dodecamer poses cannot be expected to be exhaustive, and the assignment of initial conditions is currently a limitation of our study. However, with the two force fields used we obtain a reasonable variation of poses that are well compatible with the placement of the octasaccharide, *i.e.* first two RUs. It is intuitively appealing that the ligand should settle in an elongated manner simply on account of

the geometrical constraints imposed by the unstructured loops. Releasing the restraints on the latter, nevertheless, seems to be essential. By contrast, simulations that fixated RU1 in the RU1 site showed that the ligand was unable to find an overall stable binding pose within the given simulation time (Figure S16 in the Supporting Information). Whereas the Sf6TSP-octasaccharide complexes analyzed in this work comply very well with the general observation that glycan low-energy solution conformers are recognized, MD simulation of the dodecasaccharide complex shows that the conformation of the octasaccharide subunit (RU1 and RU2) is slightly distorted, with standard deviations of the fluctuations in all glycosidic angles notably increased (*cf.* Table S3 and S4). It is therefore not surprising that in the present case both, the ligand and the protein must provide flexibility to correctly place the polysaccharide in the Sf6TSP catalytic site for cleavage. The accommodation of the dodecasaccharide may eventually be understood with a progressive conformational binding model[34], with a relaxation pathway leading through a rugged energy landscape. Furthermore, the glycan-protein contacts established by RU1 and RU3 position RU2 favorably for enzymatic cleavage, in agreement with a minimal substrate length of 3 RU. The approach used in this study, to experimentally establish a precise picture of not only glycan-protein interactions, but also glycan dynamics in the binding site could be a valuable scheme in other cases of weakly binding polysaccharide-protein complexes, where the extrapolation towards long polysaccharide fragments with computational methods is desired.

METHODS

Materials. All experiments were carried out with N-terminally shortened TSP lacking the capsid adaptor domains (ΔN, residues 109-622, M_W = 166 kDa for the native trimer).[21] LPS, polysaccharide and oligosaccharides of *S. flexneri* O-serogroup Y were obtained from Nils Carlin (Scandinavian Biopharma) and purified as described.[35]

Crystallization, data collection and structure determination. The complex of Sf6TSP E366A/D399A and octasaccharide (2RU) crystallized in space group $P2_1$ at room temperature by sitting-drop vapor-diffusion mixing 3 µl of protein solution (10 mg/ml in 10 mM sodium phosphate pH 7.5) with an equal volume of precipitant solution (0.1 M MES pH 6.5, 20 mM $MnCl_2$, 16 % w/v PEG 8000) and 0.6 µl of octasaccharide (15 mM in H_2O). Crystals appeared within two weeks, were transferred into cryo-protectant (0.1 M MES pH 6.5, 20 mM $MnCl_2$, 25 % w/v PEG 8000, 15 % w/v ethylene glycol) and frozen in liquid nitrogen. A 1.95 Å resolution data set was collected at 100 K at BL14.1 operated by the Helmholtz-Zentrum Berlin (HZB) at the BESSY II electron storage ring[36] and processed with XDS[37] and POINTLESS.[38] The crystal showed non-merohedral twinning (twinning fraction α = 0.28) and in addition, non-crystallographic translational symmetry (NCS). Initial phases were obtained by molecular replacement with Phaser[39] from the CCP4 suite[40] using the non-isomorphous structure (space group R3) of wild-type Sf6TSP bound to tetrasaccharide[22] (PDB: 2VBM). In order to minimize model bias, the initial poly-alanine model with six copies of Sf6TSP per asymmetric unit was automatically rebuilt using ARP/WARP[41]. Iterative cycles of interactive model building with COOT[42] and refinement with REFMAC5[43] and BUSTER[44] led to the final model statistics (summarized in Table S2 of the Supporting Information). Geometrical restraints used during refinement of the oligosaccharide and solvent molecules were generated with the GRADE web server (http://grade.globalphasing.org, Global Phasing Ltd.). Quality Control Check v3.0 was used for validation of the model (http://smb.slac.stanford.edu /jcsg/QC/, Joint Center for Structural Genomics). Two trimers, the functional Sf6TSP quaternary structure, were found to be generated by NCS from all six protein chains in the asymmetric unit with a rmsd of 0.22 Å for all Cα atoms. The final model coordinates have been deposited at the Protein Data Bank with accession number 4URR. Figures were generated with PyMOL.[45]

NMR spectroscopy. NMR chemical shift assignment, ^{1}H T_1 spin relaxation, ^{1}H,^{1}H transfer NOESY (trNOESY) and ^{1}H saturation transfer difference (STD) NMR experiments were performed at 56 °C on a 500 MHz Bruker Avance NMR spectrometer equipped with a TCI-Z-Gradient cryoprobe. Sf6TSP keeps its native fold at 56 °C (see Figure S17 in the Supporting Information). For octasaccharide shift assignment see Table S3. The ^{1}H,^{1}H trNOESY and ^{1}H STD NMR experiments were performed on a sample containing Sf6TSP D399N (0.12 mM) and the octasaccharide ligand (1.87 mM) in D_2O sodium phosphate buffer (100 mM, pD = 7). The 2D ^{1}H,^{1}H transfer NOESY spectrum was recorded using a phase-sensitive pulse sequence[46] with a calibrated zero quantum suppression filter[47] and a mixing time of 120 ms. A reference experiment on a sample of the ligand per se was performed to ensure the absence of NOE for the ligand in solution at this temperature.[48] Four ^{1}H STD experiments[49] were acquired with different saturation times (0.5, 1, 2 and 4 s). Saturation of the protein was achieved by irradiating on-resonance at either 7.0 or -0.4 ppm with a pulse train of 50 ms Gaussian pulses using a power level corresponding to a hard square pulse of 24 Hz; the same pulse train was irradiated off-resonance at 60 ppm as reference. STD amplification factors (STD-AF)[50] were calculated, and STD build-up curves were fitted exponentially to obtain STD-AF_0. The CORCEMA-ST-CSD analysis was conducted by altering the irradiation frequencies in intervals of 0.05 ppm using the CORCEMA-ST program.[24,51] Parameters employed in the CORCEMA-ST simulations were used as initially estimated; a free ligand correlation time of 253 ps calculated from the pulsed field gradient diffusion measurements, a correlation time of 23.9 µs when bound was calculated from the molecular mass of the protein as a trimer (165 kDa), an internal correlation time being one order of magnitude shorter[52] *i.e.* 25.3 ps, an order parameter of 0.85[53], estimated $K_A = 2000\ M^{-1}$, $k_{on} = 1{\cdot}10^7\ s^{-1}M^{-1}$, an active-site cut-off of 6 Å and $\rho_{leak} = 0.1\ s^{-1}$. Chemical shifts of the protein in the X-ray and MD molecular models were estimated by using the ShiftX2 software[54], using the ShiftY addition. In cases where the chemical shifts were not predicted by the ShiftX2 calculation, they were estimated using the predicted chemical shift of a neighboring spin. The missing chemical shift of spin i was calculated as $\delta_{calc,i} = \bar{\delta}_i + \sigma_i\left(\delta_{calc,j} - \bar{\delta}_j\right)/\sigma_j$ where $\delta_{calc,j}$ is the predicted chemical shift of the neighboring spin, $\bar{\delta}$ is the average chemical shift and σ the standard deviation of a specific atom in an amino acid (data taken from the BMRB database).[55] The transverse relaxation time ($T_{2,\mathrm{protein}}$) of Sf6TSP was estimated to 3.85 ms from a ^{1}H spectrum simulation based on the ShiftX2 chemical shifts of Sf6TSP.

Sf6TSP polysaccharide interaction analyses. LPS preparations were immobilized, and surface plasmon resonance experiments were carried out as described.[56] Protein fluorescence was measured on a Fluoromax 3 spectrofluorimeter (HORIBA Jobin Yvon, Bensheim, Germany) in PMMA poly(methyl methacrylate) cuvettes in 50 mM sodium phosphate buffer pH 7 at 184 nM TSP concentration in 3 ml test volume at 10 °C, with λ_{Ex} = 280 nm. Spectra were corrected for dilution upon polysaccharide addition. Polysaccharide binding kinetics were monitored at λ_{Em} = 336 nm, traces were fitted with a biexponential fit and k_{diss} obtained from apparent rate constants k_{app} using the relationship $k_{app} = k_{diss} + k_{ass}\cdot(c_{Polysaccharide} + c_{TSP})$ as described elsewhere.[25] The polydisperse nature of polysaccharide prevented calculation of molar concentrations and thus of k_{ass} from the data. LPS preparations were immobilized, and surface plasmon resonance experiments were carried out as described.[56] For cleavage product analysis, 1 mg/ml LPS was incubated with 20 µg/ml Sf6TSP for six days at room temperature and precipitated with 80 % (v/v) ethanol. The dried supernatant or the respective octa or dodecasaccharide controls were dissolved in 2 µL 8-aminopyrene-1,3,6-trisulfonic acid (200 mM in 15 % (v/v) acetic acid) and 2 µL sodium cyanoborohydride (1 M in tetrahydrofuran), incubated overnight at 37 °C and diluted with 96 µL water. Samples were diluted 400-fold and subjected to capillary electrophoresis as described elsewhere.[57]

Theory. All molecular dynamics (MD) simulations were carried out using the Amber force field ffo3[58] in combination with the GLYCAM parametrization for carbohydrates[32] and CHARMM36 with an improved set of carbohydrate parameters.[33,59] MD simulations were conducted in GROMACS with the TIP3P water model [tip3p].[60] Molecular topology and coordinate files for the carbohydrate were created with AmberTools using tLeap as part of Amber11[61], and then translated to GROMACS input files via a modified amb2gmx.pl.[62] After an equilibration phase, production runs between 100 and 200 ns duration at constant volume were carried out using a velocity-Verlet integrator with half-step averaged kinetic energies and a time step of 2 fs. The temperature of 310 K was maintained with a multi-chain Nose-Hoover thermostat.[63] The particle mesh Ewald (PME) method was used to calculate electrostatic interactions with a cut-off of 1.2 nm for the separation of the direct and reciprocal space summation.[64] H-bonds within water were treated with the SETTLE algorithm[65], other constraints were treated with LINCS.[66] Docking was carried out with Autodock v. 4.2.[67] Initial coordinates were obtained from the averaged saccharide structures after MD simulation with ϕ glycosidic torsions set as rigid in order to obtain rational saccharide conformations, and 100 runs were performed for each docking trial. Binding free energies were determined with the umbrella pulling procedure implemented in GROMACS as an application of the weighted histogram analysis method. [68]

ASSOCIATED CONTENT

Supporting Information

Crystal structure analysis data, NMR chemical shift assignments, STD-AF_0 data, the CORCEMA-ST-CSD approach, binding site analysis with GlyVicinityDB, fluorescence spectra, torsions in the simulation start structure, rmsd traces and snapshots of MD simulations, glycosidic torsion angles and H-bonds from molecular dynamics simulations (pdf)

This material is available free of charge via the Internet at http://pubs.acs.org.

AUTHOR INFORMATION

Corresponding Authors

*barbirz@uni-potsdam.de
*mark.santer@mpikg.mpg.de.

Present Addresses

†College of Pharmaceutical Sciences, Zhejiang University, Hangzhou, Zhejiang 310058, P.R. China
§University of Cambridge, Department of Chemistry, Cambridge, CB2 1EW, UK

Author Contributions

‡These authors contributed equally.

Notes

The authors declare no competing financial interests.

ACKNOWLEDGMENTS

The research leading to these results has received funding from the Deutsche Forschungsgemeinschaft [grant number BA 4046/1-2] to S.B., the Swedish Research Council and the Knut and Alice Wallenberg Foundation to G.W. We thank Nils Carlin (Etvax AB) for providing us with *Shigella flexneri* oligo- and polysaccharide preparations. We thank Sebastian Mahlow for assistance with CE-LIF and Mandy Schietke for excellent technical assistance. We thank the staff at BESSY II (Helmholtz-Zentrum Berlin) for support with diffraction experiments and Manfred Weiss for helpful discussions on data processing.

REFERENCES

(1) Whitfield, C.; Trent, M. S. Biosynthesis and Export of Bacterial Lipopolysaccharides. *Annu Rev Biochem* **2014,** *83*, 99.

(2) Mazmanian, S. K.; Liu, C. H.; Tzianabos, A. O.; Kasper, D. L. An immunomodulatory molecule of symbiotic bacteria directs maturation of the host immune system. *Cell* **2005,** *122* (1), 107.

(3) Steinberg, N.; Kolodkin-Gal, I. The Matrix Reloaded: How Sensing the Extracellular Matrix Synchronizes Bacterial Communities. *J Bacteriol* **2015,** *197* (13), 2092.

(4) Zimmermann, S.; Lepenies, B. In *Carbohydrate-Based vaccines: Methods and Protocols*; Lepenies, B., Ed. Clifton, NJ, 2015; Vol. 1331.

(5) Kuttel, M. M.; Jackson, G. E.; Mafata, M.; Ravenscroft, N. Capsular polysaccharide conformations in pneumococcal serotypes 19F and 19A. *Carbohyd Res* **2015,** *406*, 27.

(6) Haji-Ghassemi, O.; Blackler, R. J.; Martin Young, N.; Evans, S. V. Antibody recognition of carbohydrate epitopes. *Glycobiology* **2015,** *25* (9), 920.

(7) Little, D. J.; Li, G.; Ing, C.; DiFrancescoc, B. R.; Bamford, N. C.; Robinson, H.; Nitz, M.; Pomes, R.; Howell, P. L. Modification and periplasmic translocation of the biofilm exopolysaccharide poly-beta-1,6-N-acetyl-D-glucosamine. *P Natl Acad Sci U S A* **2014,** *111* (30), 11013.

(8) Vulliez-Le Normand, B.; Saul, F. A.; Phalipon, A.; Belot, F.; Guerreiro, C.; Mulard, L. A.; Bentley, G. A. Structures of synthetic O-antigen fragments from serotype 2a Shigella

flexneri in complex with a protective monoclonal antibody. *Proc Natl Acad Sci U S A* **2008,** *105* (29), 9976.
(9) Battistel, M. D.; Shangold, M.; Trinh, L.; Shiloach, J.; Freedberg, D. I. Evidence for Helical Structure in a Tetramer of alpha 2-8 Sialic Acid: Unveiling a Structural Antigen. *J Am Chem Soc* **2012,** *134* (26), 10717.
(10) Woods, R. J.; Tessier, M. B. Computational glycoscience: characterizing the spatial and temporal properties of glycans and glycan-protein complexes. *Curr Opin Struc Biol* **2010,** *20* (5), 575.
(11) Widmalm, G. A perspective on the primary and three-dimensional structures of carbohydrates. *Carbohyd Res* **2013,** *378*, 123.
(12) Andres, D.; Baxa, U.; Hanke, C.; Seckler, R.; Barbirz, S. Carbohydrate binding of Salmonella phage P22 tailspike protein and its role during host cell infection. *Biochem Soc Trans* **2010,** *038* (5), 1386.
(13) Steinbacher, S.; Baxa, U.; Miller, S.; Weintraub, A.; Seckler, R.; Huber, R. Crystal structure of phage P22 tailspike protein complexed with Salmonella sp. O-antigen receptors. *Proc Natl Acad Sci U S A* **1996,** *93* (20), 10584.
(14) Schulz, E. C.; Schwarzer, D.; Frank, M.; Stummeyer, K.; Muhlenhoff, M.; Dickmanns, A.; Gerardy-Schahn, R.; Ficner, R. Structural Basis for the Recognition and Cleavage of Polysialic Acid by the Bacteriophage K1F Tailspike Protein EndoNF. *J Mol Biol* **2010,** *397* (1), 341.
(15) Barry, E. M.; Pasetti, M. F.; Sztein, M. B.; Fasano, A.; Kotloff, K. L.; Levine, M. M. Progress and pitfalls in Shigella vaccine research. *Nat Rev Gastro Hepat* **2013,** *10* (4), 245.
(16) Jonsson, K. H. M.; Sawen, E.; Widmalm, G. Studies on the conformational flexibility of alpha-L-rhamnose-containing oligosaccharides using C-13-site-specific labeling, NMR spectroscopy and molecular simulations: implications for the three-dimensional structure of bacterial rhamnan polysaccharides. *Org Biomol Chem* **2012,** *10* (12), 2453.
(17) Kang, Y.; Barbirz, S.; Lipowski, R.; Santer, M. Conformational Diversity of O-antigen Polysaccharides of the Gram-negative Bacterium Shigella flexneri Serotype Y. *J Phys Chem B* **2014,** *118*, 2523.
(18) West, N. P.; Sansonetti, P.; Mounier, J.; Exley, R. M.; Parsot, C.; Guadagnini, S.; Prévost, M. C.; Prochnicka-Chalufour, A.; Delepierre, M.; Tanguy, M.et al. Optimization of virulence functions through glucosylation of Shigella LPS. *Science* **2005,** *307* (5713), 1313.
(19) Simmons, D. A. R.; Romanowska, E. Structure and biology of *Shigella flexneri* O-antigens. *J Med Microbiol* **1987,** *23* (4), 289.
(20) Lindberg, A. A.; Wollin, R.; Gemski, P.; Wohlhieter, J. A. Interaction between bacteriophage Sf6 and *Shigella flexneri*. *J Virol* **1978,** *27* (1), 38.
(21) Freiberg, A.; Morona, R.; Van den Bosch, L.; Jung, C.; Behlke, J.; Carlin, N.; Seckler, R.; Baxa, U. The tailspike protein of Shigella phage Sf6 - A structural homolog of Salmonella phage p22 tailspike protein without sequence similarity in the beta-helix domain. *J Biol Chem* **2003,** *278* (3), 1542.
(22) Muller, J. J.; Barbirz, S.; Heinle, K.; Freiberg, A.; Seckler, R.; Heinemann, U. An intersubunit active site between supercoiled parallel beta helices in the trimeric tailspike endorhamnosidase of Shigella flexneri Phage Sf6. *Structure* **2008,** *16* (5), 766.
(23) Dixon, A. M.; Venable, R.; Widmalm, G.; Bull, T. E.; Pastor, R. W. Application of NMR, molecular simulation, and hydrodynamics to conformational analysis of trisaccharides. *Biopolymers* **2003,** *69* (4), 448.
(24) Jayalakshmi, V.; Krishna, N. R. Complete relaxation and conformational exchange matrix (CORCEMA) analysis of intermolecular saturation transfer effects in reversibly forming ligand-receptor complexes. *J Magn Reson* **2002,** *155* (1), 106.
(25) Baxa, U.; Cooper, A.; Weintraub, A.; Pfeil, W.; Seckler, R. Enthalpic barriers to the hydrophobic binding of oligosaccharides to phage P22 tailspike protein. *Biochemistry* **2001,** *40* (17), 5144.
(26) McNamara, J. T.; Morgan, J. L. W.; Zimmer, J. A Molecular Description of Cellulose Biosynthesis. *Annu Rev Biochem* **2015,** *84*, 895.
(27) Woodward, R.; Yi, W.; Li, L.; Zhao, G.; Eguchi, H.; Sridhar, P. R.; Guo, H.; Song, J. K.; Motari, E.; Cai, L.et al. In vitro bacterial polysaccharide biosynthesis: defining the functions of Wzy and Wzz. *Nat Chem Biol* **2010,** *6* (6), 418.
(28) Ruiz, N.; Kahne, D.; Silhavy, T. J. TIMELINE Transport of lipopolysaccharide across the cell envelope: the long road of discovery. *Nat Rev Microbiol* **2009,** *7* (9), 677.
(29) Kadirvelraj, R.; Gonzalez-Outeirino, J.; Foley, B. L.; Beckham, M. L.; Jennings, H. J.; Foote, S.; Ford, M. G.; Woods, R. J. Understanding the bacterial polysaccharide antigenicity of Streptococcus agalactiae versus Streptococcus pneumoniae. *Proc Natl Acad Sci U S A* **2006,** *103* (21), 8149.
(30) Parent, K. N.; Erb, M. L.; Cardone, G.; Nguyen, K.; Gilcrease, E. B.; Porcek, N. B.; Pogliano, J.; Baker, T. S.; Casjens, S. R. OmpA and OmpC are critical host factors for bacteriophage Sf6 entry in Shigella. *Mol Microbiol* **2014,** *92* (1), 47.
(31) Theillet, F. X.; Frank, M.; Normand, B. V. L.; Simenel, C.; Hoos, S.; Chaffotte, A.; Belot, F.; Guerreiro, C.; Nato, F.; Phalipon, A.et al. Dynamic aspects of antibody: oligosaccharide complexes characterized by molecular dynamics simulations and saturation transfer difference nuclear magnetic resonance. *Glycobiology* **2011,** *21* (12), 1570.
(32) Kirschner, K. N.; Yongye, A. B.; Tschampel, S. M.; Gonzalez-Outeirino, J.; Daniels, C. R.; Foley, B. L.; Woods, R. J. GLYCAM06: A generalizable Biomolecular force field. Carbohydrates. *J Comput Chem* **2008,** *29* (4), 622.
(33) Guvench, O.; Hatcher, E.; Venable, R. M.; Pastor, R. W.; MacKerell, A. D., Jr. CHARMM Additive All-Atom Force Field for Glycosidic Linkages between Hexopyranoses. *J Chem Theory Comput* **2009,** *5* (9), 2353.
(34) Bras, N. F.; Cerqueira, N. M. F. S. A.; Fernandes, P. A.; Ramos, M. J. Carbohydrate-binding modules from family 11: Understanding the binding mode of polysaccharides. *Int J Quantum Chem* **2008,** *108* (11), 2030.
(35) Darveau, R. P.; Hancock, R. E. Procedure for isolation of bacterial lipopolysaccharides from both smooth and rough Pseudomonas aeruginosa and Salmonella typhimurium strains. *J Bacteriol* **1983,** *155* (2), 831.
(36) Mueller, U.; Darowski, N.; Fuchs, M. R.; Foerster, R.; Hellmig, M.; Paithankar, K. S.; Puehringer, S.; Steffien, M.; Zocher, G.; Weiss, M. S. Facilities for macromolecular crystallography at the Helmholtz-Zentrum Berlin. *J Synchrotron Radiat* **2012,** *19*, 442.
(37) Krug, M.; Weiss, M.; Heinemann, U.; Mueller, U. XDSAPP: a graphical user interface for the convenient processing of diffraction data using XDS. *J Appl Cryst* **2012,** *45*, 568.
(38) Evans, P. Scaling and assessment of data quality. *Acta Crystallogr D* **2006,** *62*, 72.
(39) McCoy, A. J.; Grosse-Kunstleve, R. W.; Adams, P. D.; Winn, M. D.; Storoni, L. C.; Read, R. J. Phaser crystallographic software. *J Appl Crystallogr* **2007,** *40* (Pt 4), 658.
(40) Bailey, S. The Ccp4 Suite - Programs for Protein Crystallography. *Acta Crystallogr D* **1994,** *50*, 760.
(41) Langer, G.; Cohen, S.; Lamzin, V.; Perrakis, A. Automated macromolecular model building for X-ray crystallography using ARP/wARP version 7. *Nat Protoc* **2008,** *3* (7), 1171.
(42) Emsley, P.; Cowtan, K. Coot: model-building tools for molecular graphics. *Acta Crystallogr D* **2004,** *60* (Pt 12 Pt 1), 2126.

(43) Murshudov, G. N.; Vagin, A. A.; Dodson, E. J. Refinement of macromolecular structures by the maximum-likelihood method. *Acta Crystallogr D* **1997,** *53* (Pt 3), 240.
(44) Bricogne, G.; Blanc, E.; Brandl, M.; Flensburg, C.; Keller, P.; Paciorek, W.; Roversi, P.; Sharff, A.; Smart, O. S.; Vonrhein, C.et al.; Global Phasing Ltd.: Cambridge, United Kingdom, 2011.
(45) SchroedingerLLC, 2015.
(46) Wagner, R.; Berger, S. Gradient-selected NOESY - A fourfold reduction of the measurement time for the NOESY experiment. *J Magn Reson* **1996,** *123* (1), 119.
(47) Thrippleton, M. J.; Keeler, J. Elimination of zero-quantum interference in two-dimensional NMR spectra. *Angew Chem Int Edit* **2003,** *42* (33), 3938.
(48) Landstroem, J.; Nordmark, E. L.; Eklund, R.; Weintraub, A.; Seckler, R.; Widmalm, G. Interaction of a Salmonella enteritidis O-antigen octasaccharide with the phage P22 tailspike protein by NMR spectroscopy and docking studies. *Glycoconjugate J* **2008,** *25* (2), 137.
(49) Mayer, M.; Meyer, B. Characterization of ligand binding by saturation transfer difference NMR spectroscopy. *Angew Chem Int Edit* **1999,** *38* (12), 1784.
(50) Mayer, M.; Meyer, B. Group epitope mapping by saturation transfer difference NMR to identify segments of a ligand in direct contact with a protein receptor. *J Am Chem Soc* **2001,** *123* (25), 6108.
(51) Krishna, N.; Jayalakshmi, V. Complete relaxation and conformational exchange matrix analysis of STD-NMR spectra of ligand-receptor complexes. *Prog Nucl Mag Res Sp* **2006,** *49* (1), 1.
(52) Rundlöf, T.; Venable, R. M.; Pastor, R. W.; Kowalewski, J.; Widmalm, G. Distinguishing anisotropy and flexibility of the pentasaccharide LNF-1 in solution by carbon-13 NMR relaxation and hydrodynamic modeling. *J Am Chem Soc* **1999,** *121* (50), 11847.
(53) Jayalakshmi, V.; Krishna, N. R. Determination of the conformation of trimethoprim in the binding pocket of bovine dihydrofolate reductase from a STD-NMR intensity-restrained CORCEMA-ST optimization. *J Am Chem Soc* **2005,** *127* (40), 14080.
(54) Han, B.; Liu, Y.; Ginzinger, S. W.; Wishart, D. S. SHIFTX2: significantly improved protein chemical shift prediction. *J Biomol NMR* **2011,** *50* (1), 43.
(55) Ulrich, E. L.; Akutsu, H.; Doreleijers, J. F.; Harano, Y.; Ioannidis, Y. E.; Lin, J.; Livny, M.; Mading, S.; Maziuk, D.; Miller, Z.et al. BioMagResBank. *Nucleic Acids Res* **2008,** *36*, D402.
(56) Andres, D.; Roske, Y.; Doering, C.; Heinemann, U.; Seckler, R.; Barbirz, S. Tail morphology controls DNA release in two Salmonella phages with one lipopolysaccharide receptor recognition system. *Mol Microbiol* **2012,** *83* (6), 1244.
(57) Malinova, I.; Mahlow, S.; Alseekh, S.; Orawetz, T.; Fernie, A. R.; Baumann, O.; Steup, M.; Fettke, J. Double Knockout Mutants of Arabidopsis Grown under Normal Conditions Reveal that the Plastidial Phosphorylase Isozyme Participates in Transitory Starch Metabolism. *Plant Physiol* **2014,** *164* (2), 907.
(58) Duan, Y.; Wu, C.; Chowdhury, S.; Lee, M. C.; Xiong, G. M.; Zhang, W.; Yang, R.; Cieplak, P.; Luo, R.; Lee, T.et al. A point-charge force field for molecular mechanics simulations of proteins based on condensed-phase quantum mechanical calculations. *J Comput Chem* **2003,** *24* (16), 1999.
(59) Klauda, J. B.; Venable, R. M.; Freites, J. A.; O'Connor, J. W.; Tobias, D. J.; Mondragon-Ramirez, C.; Vorobyov, I.; MacKerell, A. D., Jr.; Pastor, R. W. Update of the CHARMM All-Atom Additive Force Field for Lipids: Validation on Six Lipid Types. *J Phys Chem B* **2010,** *114* (23), 7830.
(60) Van der Spoel, D.; Lindahl, E.; Hess, B.; Groenhof, G.; Mark, A. E.; Berendsen, H. J. C. GROMACS: Fast, flexible, and free. *J Comput Chem* **2005,** *26* (16), 1701.
(61) Case, D. A.; Darden, T. A.; Cheatham III, T. E.; Simmerling, C. L.; Wang, J.; Duke, R. E.; Luo, R.; Walker, R. C.; Zhang, W.; Merz, K. M.et al.; University of California, San Francisco, 2010.
(62) Wehle, M.; Vilotijevic, I.; Lipowsky, R.; Seeberger, P. H.; Silva, D. V.; Santer, M. Mechanical Compressibility of the Glycosylphosphatidylinositol (GPI) Anchor Backbone Governed by Independent Glycosidic Linkages. *J Am Chem Soc* **2012,** *134* (46), 18964.
(63) Martyna, G. J.; Klein, M. L.; Tuckerman, M. Nosé-Hoover chains: The canonical ensemble via continuous dynamics. *J Chem Phys* **1992,** *97* (4), 2635.
(64) Darden, T.; York, D.; Pedersen, L. Particle mesh Ewald: An *N*-log(*N*) Method for Ewald Sums in Large Systems. *J Chem Phys* **1993,** *98* (12), 10089.
(65) Miyamoto, S.; Kollman, P. A. SETTLE: An Analytical Version of the SHAKE and RATTLE Algorithms for Rigid Water Models. *J Comput Chem* **1992,** *13* (8), 952.
(66) Hess, B.; Bekker, H.; Berendsen, H. J. C.; Fraaije, J. LINCS: A linear constraint solver for molecular simulations. *J Comput Chem* **1997,** *18* (12), 1463.
(67) Morris, G. M.; Huey, R.; Lindstrom, W.; Sanner, M. F.; Belew, R. K.; Goodsell, D. S.; Olson, A. J. AutoDock4 and AutoDockTools4: Automated Docking with Selective Receptor Flexibility. *J Comput Chem* **2009,** *30* (16), 2785.
(68) Kumar, S.; Bouzida, D.; Swendsen, R. H.; Kollman, P. A.; Rosenberg, J. M. The Weighted Histogram Analysis Method for Free-Energy Calculations on Biomolecules. I. The Method. *J Comput Chem* **1992,** *13* (8), 1011.

Table of Contents artwork